

Estimation of the Mass of the Very Massive Galaxy Cluster SRGe CL2305.2-2248 from Strong Lensing

I. M. Khamitov^{1,2*}, I. F. Bikmaev^{2,3,4}, N. S. Lyskova^{5,6}, A. A. Kruglov⁵, R. A. Burenin^{4,5},
M. R. Gilfanov^{5,7}, A. A. Grokhovskaya^{8,9}, S. N. Dodonov^{4,8,9}, S. Yu. Sazonov⁵,
A. A. Starobinsky¹⁰, R. A. Sunyaev^{5,7}, I. I. Khabibullin^{5,7,11}, and E. M. Churazov^{5,7}

¹*TÜBITAK National Observatory, Antalya, Turkey*

²*Kazan Federal University, Kazan, 420000 Russia*

³*Academy of Sciences of Tatarstan, Kazan, Russia*

⁴*Sternberg Astronomical Institute,
Moscow State University, Moscow, 119234 Russia*

⁵*Space Research Institute, Russian Academy of Sciences, Moscow, 117997 Russia*

⁶*Astrospace Center, Lebedev Physical Institute, Russian Academy of Sciences, Moscow, 117997 Russia*

⁷*Max Planck Institut für Astrophysik, Karl-Schwarzschild-Str. 1, Postfach 1317, D-85741 Garching, Germany*

⁸*Special Astrophysical Observatory, Russian Academy of Sciences, Nizhnii Arkhyz, Karachai-Cherkessian
Republic, 369167 Russia*

⁹*Institute of Applied Astronomy, Russian Academy of Sciences, St. Petersburg, 191187 Russia*

¹⁰*Landau Institute for Theoretical Physics, Russian Academy of Sciences, Chernogolovka, Russia*

¹¹*Ludwig-Maximilians-Universität München, München, Germany*

Received December 1, 2021; revised December 3, 2021; accepted December 3, 2021

Abstract—SRGe CL2305.2–2248 (SPT-CL J2305–2248, ACT-CL J2305.1–2248) is one of the most massive galaxy clusters at high redshifts ($z \simeq 0.76$) and is of great interest for cosmology. Deep images have been obtained at the Russian–Turkish 1.5-m telescope (RTT-150) for an optical identification of this cluster. In combination with the open Hubble Space Telescope archival data, they have made it possible to select candidates for gravitationally lensed images of distant blue galaxies in the form of arcs and arclets. The observed giant arc near the brightest cluster galaxies allows the Einstein radius to be estimated, 9.8 ± 1.3 arcsec. The photometric redshift of the lensed source has been found ($z_s = 2.44 \pm 0.07$). Its use in combination with the Einstein radius estimate has made it possible to independently estimate the mass of SRGe CL2305.2–2248 by extrapolating the strong-lensing results to large radii and using model density profiles in relaxed clusters. This extrapolation leads to mass estimates smaller than those obtained from X-ray and microwave observations by a factor of ~ 1.5 – 3 . A probable cause of this discrepancy may be the galaxy merger process, which is also confirmed by the morphology of SRGe CL2305.2–2248 in the optical range.

DOI: 10.1134/S1063773722010042

Keywords: *galaxy clusters, galaxy cluster SRGe CL2305.2-2248, strong lensing.*

INTRODUCTION

The very massive galaxy cluster SRGe CL2305.2–2248 was detected in X-rays based on the results of the first all-sky survey with the eROSITA telescope onboard the SRG space observatory (Predehl et al., 2021, Sunyaev et al., 2021), which was completed in June 2020. Based on the results of optical observations at the Russian–Turkish 1.5-m telescope

(RTT-150) and the 6-m BTA telescope, we performed an optical identification of the cluster and obtained a spectroscopic redshift measurement for the cluster, $z = 0.7573$ (Burenin et al. 2021). The presence of strong gravitational lensing in the cluster field is noted in Table 8 from the paper by Bleem et al. (2020) on the early detection of this cluster (SPT-CL J2305–2248) in the millimeter band of the South Pole Telescope survey. In this paper we made a photometric redshift estimate for the

*E-mail: irek_khamitov@hotmail.com

Table 1. Log of observations of SRGe CL2305.2–2248 at RTT-150

Date	F , SDSS	N	T , s	σ , arcsec
Aug. 23, 2020	g	4	2400	2.4
Aug. 23, 2020	r	4	2400	2.0
Aug. 23, 2020	i	4	2400	1.7
Aug. 23, 2020	z	4	2400	1.7
Aug. 24, 2020	g	4	2400	1.6
Aug. 24, 2020	r	4	2400	1.7
Aug. 24, 2020	i	4	2400	1.6
Aug. 24, 2020	z	5	3000	1.6
Aug. 25, 2020	g	4	2400	2.0
Aug. 25, 2020	r	5	3000	2.2
Aug. 25, 2020	i	6	3600	2.1
Aug. 25, 2020	z	5	3000	2.0
Aug. 26, 2020	g	10	6000	2.0
Aug. 26, 2020	r	10	6000	2.2

F is the SDSS filter, N is the number of images, T is the total exposure time in seconds, and σ is the seeing in arcsec.

lensed source and obtained an independent estimate of the cluster mass in the Einstein ring. When approximating the cluster mass to distance R_{500} , we considered the Navarro–Frenk–White model density profile (Navarro et al. 1996). In our estimates we assume a standard Λ CDM cosmological model with the following parameters: $\Omega_m = 0.3$, $\Omega_\Lambda = 0.7$, and $H_0 = 70 \text{ km s}^{-1} \text{ Mpc}^{-1}$.

PHOTOMETRIC OBSERVATIONS

Deep direct images of the field of the galaxy cluster SRGe CL2305.2–2248 were obtained at the Russian–Turkish 1.5-m telescope (RTT-150) within the ground support of the X-ray survey with the eROSITA telescope onboard the Spectrum–Roentgen–Gamma (SRG) space observatory. The

observations were carried out by using TFOSC instrument from August 23 to 26, 2020, in the SDSS g , r , i , and z filters. An Andor iKon-L 936 BEX2-DD-9ZQ 2048×2048 -pixel CCD camera with a resolution of $0''.326$ per pixel was used as a detector. The quantum efficiency of the CCD detector is $\sim 90\%$ or higher in the wavelength range from 4000 to 8500 Å. A log of our observations is given in Table 1. The total moderate-quality exposure times were 13 200, 13 800, 8400, and 8400 s in the SDSS g , r , i , and z filters, respectively. The total exposure time in each filter was divided into 600-s exposure times between which the telescope pointing axis was shifted by $10''$ – $20''$ in an arbitrary direction. The direct images were reduced in a standard way using the IRAF package and our own software with the application of a standard set of calibrations.

Photometric calibration of the images was obtained using the observations of photometric standards (Smith et al. 2002).

SELECTION OF LENSED IMAGES

Deep images with a limiting magnitude as faint as 23–24 in the four g , r , i , and z filters of the SDSS photometric system were obtained at RTT-150 for an optical identification of the cluster under study. At $z = 0.76$ the main flux from the cluster galaxies falls into the i and z filters. The images in the g and r filters were used to cut off the background galaxies at lower redshifts. The number of background galaxies that were distinguished by $(g - r)$ and $(r - i)$ colors in the RTT-150 images and that did not belong to the cluster in a 9×9 -arcmin field was ~ 1000 . An analysis of the images showed that, in addition to the large number of background galaxies detected in all g , r , and i filters in regions close in position to two brightest cluster galaxies (BCG), about ten blue sources visible only in the g filter are detected. Since the presence of strong gravitational lensing in the cluster field was noted in Bleem et al. (2020), we suggested that the blue sources in the RTT-150 frames near the BCG could be associated with gravitational lensing features (arcs). To select the lensed images of a distant source, we used deep RTT-150 images of the cluster field in the g , r , i , and z bands and high-spatial-resolution images from the open Hubble Space Telescope (HST) archive (Whitmore et al. 2016) taken on April 23, 2018, in the F110W filter with the WFC3/IR detector, an exposure time of 758.81 s (Fig. 1), and in the F200LP filter with the WFC3/UVIS detector, an exposure time of 741 s.

The lensed candidates were selected by source morphology in the HST image and by brightness excess in the g band compared to the r , i , and z bands.

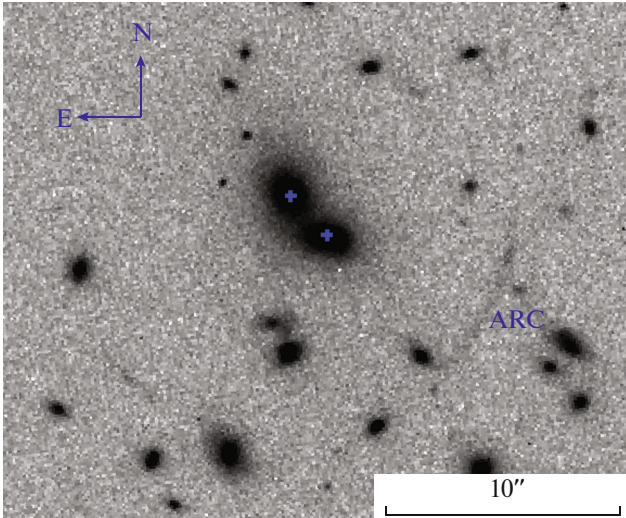


Fig. 1. HST image of the cluster field. The positions of the centers of the two brightest cluster galaxies are marked.

The selected candidates in the form of arcs and arclets are marked in Fig. 2. The brightness of the sources in close to the detection limit in the g image and is $\sim 24^m$. The observed giant arc near the brightest cluster galaxies was detected in the g image in the form of three separate sources. The arc lies virtually on one circumference together with two sources southeastward (concentrically matched with the arc in the HST image), suggesting a high degree of circular symmetry of the lens and its excellent position on the line of sight between the observer and the lensed galaxy. Thus, when estimating the mass of the lens, we may consider a concentrically symmetric 2D distribution of its mass. Figure 3 shows this region in the g , r , i , and z bands. The blue and red circles indicate the fits to the Einstein ring obtained, respectively, by analyzing the HST image of the arc and the southeastern arclets and the identified sources based on RTT-150 data. The circumference radius determines the angular distance Θ_{arc} corresponding to the Einstein radius. The centers of the circumferences are also marked: from HST (blue) and RTT-150 (red) data. The radii of the circumferences and their centers are seen to be in good agreement with each other. Thus, we showed the possibility of using RTT-150 in estimates of this kind. We took the distance between the circumference center and the BCG, $1''.3$, as the error of Θ_{arc} in this system.

ESTIMATION OF THE LENS REDSHIFT

The total exposure times for the deep fields in the g and r bands are the same. Consequently, taking into account the same detector quantum efficiency and filter transmission in these bands, the depth of the fields

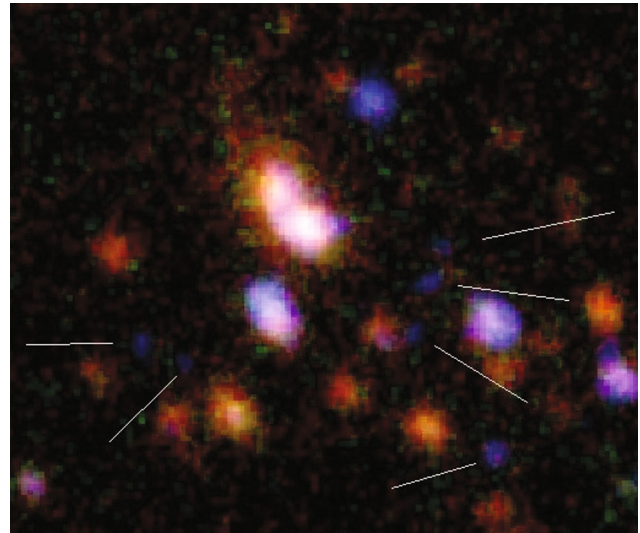


Fig. 2. The color image of the cluster field formed from RTT-150 data in the g , r , and i bands. The selected blue sources in the form of arcs and arclets in the HST image are marked.

is also approximately the same. The absence of a signal in the r , i , and z bands allowed us to constrain the redshift of the lensed source. With a great probability this is a galaxy with intense star formation. Therefore, the signal detected in the g band corresponds to the fall of the L_{α} (1215 \AA) emission line into this spectral region. The strong C IV (1549 \AA) line must also fall into the same region; otherwise the signal from it would be detected in the r band. C IV cannot be the only line falling into the g band either. In this case, a strong Mg II (2799 \AA) emission line would be detected in the i band. From these considerations and by analyzing the transmission function of the g filter used at RTT-150, we determined the upper and lower redshift limits for the lensed galaxy. In Fig. 4 the red dashed line indicates the wavelength region of the L_{α} line position for the distant source, when the L_{α} and C IV lines simultaneously fall into this band. When estimating the wavelength range, we considered the filter transmission above 70%.

Thus, we determined the redshift of the lensed source, $z_s = 2.44 \pm 0.07$, which was used to estimate the mass.

ESTIMATION OF THE MASS FROM STRONG GRAVITATIONAL LENSING

In this paper we used the same approach to estimating the mass as that in Dahle et al. (2016) for the cluster PSZ1 G311.65-18.48 discovered by the Planck observatory, with a gravitationally lensed image of a distant galaxy in the form of a giant arc having been detected in its field. The parameters of the lensed

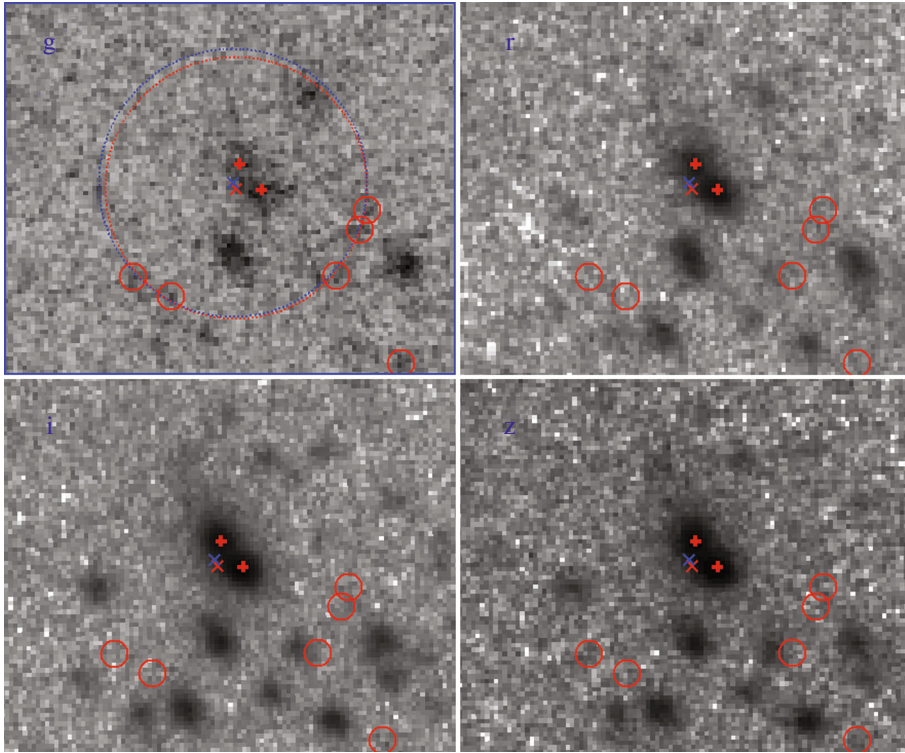


Fig. 3. Deep g , r , i , and z images of the $30'' \times 30''$ region around the BCG. The red crosses mark the positions of the two brightest cluster galaxies.

system (the Einstein radius in angular, Θ_{arc} , and physical, R_{Ein} , units, the source and lens redshifts, and the corresponding angular diameter distances¹) to calculate the mass are given in Table 2.

The cluster mass within the cylinder of radius $R_{\text{Ein}} = 72.2$ kpc is estimated to be

$$M_{\text{Ein}}^{\text{cyl}} = \pi R_{\text{Ein}}^2 \Sigma_{\text{crit}} = 3.3_{-0.8}^{+0.95} \times 10^{13} M_{\odot}, \quad (1)$$

where Σ_{crit} is the critical surface density (Eq. (4) in the Appendix).

The cluster mass estimate $M_{500} \sim 9.03 \times 10^{14} M_{\odot}$ in Burenin et al. (2021) implies that the radius of the sphere inside which the mean density exceeds the critical density at $z = 0.7573$ by a factor of 500 is $R_{500}^X \sim 1110$ kpc, corresponding to an angular size $\sim 2'.5$. Thus, to recalculate the mass determined from strong lensing to $M(<R_{500}^X)$, we need an extrapolation in radius by a factor $R_{500}^X/R_{\text{Ein}} \sim 15$, which limits the accuracy of such calculations.

The cluster mass within the sphere of radius R_{500}^X can be roughly estimated by assuming that the lensing cluster is described by the model of an isothermal

sphere with a density profile $\rho(r) \propto r^{-\gamma}$, where $\gamma = 2$, by analogy with the calculations performed for elliptical galaxies in Lyskova et al. (2018). For a given γ the mass (1) within the cylinder of radius R_{Ein} can

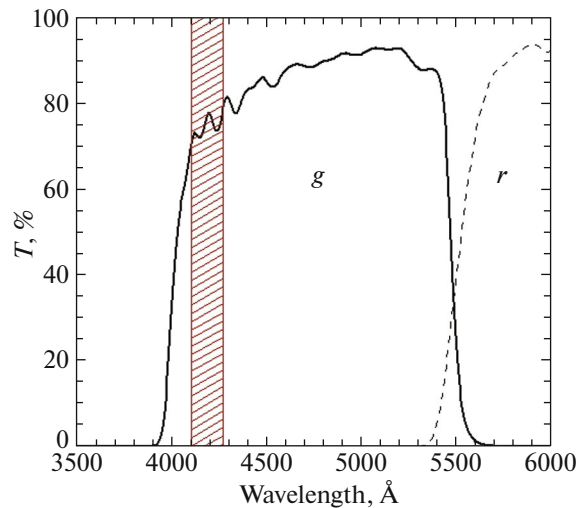


Fig. 4. Transmission of the g filter used at RTT-150. The wavelength region of the L_{α} line position for the distant source, when the L_{α} and C IV lines simultaneously fall into this band, is marked.

¹The angular diameter distance is defined as the ratio of the object's diameter in physical units to its angular size in radians.

Table 2. Parameters of the gravitationally lensed system

Parameters	Values
Θ_{arc} , arcsec	9.8 ± 1.3
R_{Ein} , kpc	72.2 ± 9.6
z_d	0.7573 ± 0.0006
z_s	2.44 ± 0.07
D_d , Mpc	1519 ± 0.44
D_s , Mpc	$1674_{-9.9}^{+9.6}$

The Einstein radius in angular, Θ_{arc} , and physical, R_{Ein} , units, the source, z_s , and lens, z_d , redshifts, and the corresponding angular diameter distances D_s and D_d .

be recalculated to the mass within the sphere of the same radius. For $\gamma = 2$ this mass is $2 \times 10^{13} M_{\odot}$. In that case, the cluster mass within the sphere of radius 1110 kpc is $M = (3.3 \pm 0.4) \times 10^{14} M_{\odot}$, which is lower than the mass derived from the mass–X-ray luminosity relation in Burenin et al. (2021) by a factor ~ 3 .

Undoubtedly, the assumption about the slope $\gamma = 2$ over the entire range of radii from $\sim 0.07 R_{500}^X$ to R_{500}^X is a rough approximation of the actually observed density profiles that can be used only for order-of-magnitude estimates. The fits by the Navarro–Frenk–White (Navarro et al. 1996) or Einasto (Einasto 1965) profiles, which describe well the numerical cluster formation simulations when the contribution of ordinary matter (baryons) may be neglected, are a better approximation. In the case of the slightly simpler Navarro–Frenk–White profile, the slope of the density profile changes from $\gamma = 1$ at small radii to $\gamma = 3$ at large ones.

Let us estimate the cluster mass by assuming that the density is specified by the Navarro–Frenk–White model:

$$\rho(r) = \frac{\delta_c \rho_{\text{crit}}}{\left(\frac{r}{R_s}\right) \left(1 + \frac{r}{R_s}\right)^2}, \quad (2)$$

where $\rho_{\text{crit}} = 3H^2(z)/(8\pi G)$ is the critical density, $H(z) = H_0(\Omega_m(1+z)^3 + \Omega_{\Lambda})^{1/2}$ is the Hubble constant at the cluster redshift, and G is the gravitational constant. The characteristic cluster radius is $R_s = R_{200}/c$, where c is the dimensionless concentration

that enters into the density profile normalization as

$$\delta_c = \frac{200}{3} \frac{c^3}{\ln(1+c) - c/(1+c)}. \quad (3)$$

The cluster size R_{200} is defined as the radius of the sphere within which the mean halo density is $200\rho_{\text{crit}}$. Accordingly, the halo mass is $M_{200} \equiv M(R_{200}) = \frac{4}{3}\pi R_{200}^3 \times 200\rho_{\text{crit}}$.

As studies of the properties of dark matter halos in numerical simulations show (see, e.g., Duffy et al. 2008), the parameters c and M_{200} are closely correlated in a wide range of halo masses. For further estimates we use the halo concentration–mass (given the cluster redshift) relation from Duffy et al. (2008). Thus, only one free parameter, the halo mass, remains in the Navarro–Frenk–White model. For a spherically symmetric lens the tangential arc must be close in position to the tangential critical curve (the properties of a lens with the Navarro–Frenk–White density profile are described in Bartelmann (1996), see also the Appendix). By setting Θ_{arc} equal to the size of the critical curve in the lens plane, we obtain an independent estimate for the halo mass. Within the above-described assumptions the best agreement with the observed position of the arc is achieved at $M_{200} = 7.1 \times 10^{14} M_{\odot}$ ($R_{200} = 1388$ kpc). In this case, the concentration is $c = 3.8$ and $R_s = R_{200}/c = 365$ kpc. Thus, for comparison with the mass estimates obtained from X-ray data and the Sunyaev–Zeldovich effect, we can calculate the mass of the dark matter halo $M_{500} = (4.9 \pm 0.7) \times 10^{14} M_{\odot}$ within the radius inside which the mean halo density is $500\rho_{\text{crit}}$ ($z = 0.7573$) and the mass within $R_{500}^X = 1110$ kpc, which is $M(<R_{500}^X) = (5.9 \pm 0.6) \times 10^{14} M_{\odot}$. The errors in the mass were derived from the uncertainty in the position of the halo center, i.e., the center of the circumference (Fig. 3). The radius of the tangential critical curve for the Navarro–Frenk–White profile is plotted against the dark halo mass $M(<R_{500}^X)$ in Fig. 5. The mass estimate that agrees best with the position of the tangential arc is marked by the gray cross. The cluster mass found by Burenin et al. (2021) from X-ray observations within the SRG/eROSITA survey and corresponding to $R_{500}^X = 1110$ kpc is also shown for comparison. The currently available estimates of the mass M_{500} (the physical size of the sphere within which the mass was determined can be different for different methods) for the cluster SRGe CL2305.2-2248 are collected in Table 3. As follows from Table 3 and Fig. 5, the cluster mass estimated from gravitational lensing is less than the mass from the literature by a factor of ~ 1.5 – 2 .

It is worth noting that the size of the critical curve depends significantly on the derivative of the

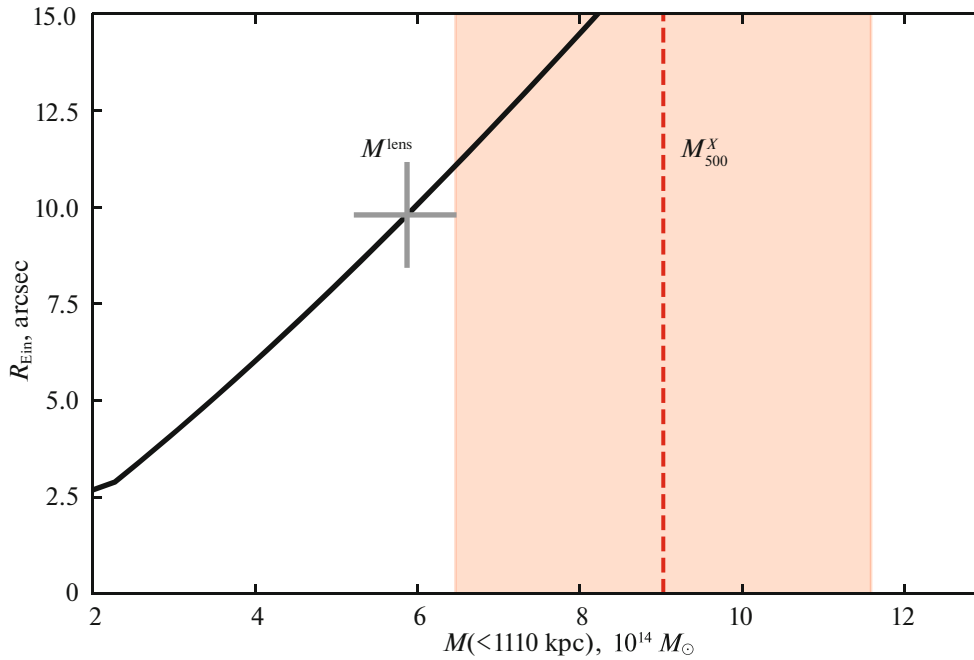


Fig. 5. Size of the tangential critical curve for a spherically symmetric Navarro–Frenk–White profile versus cluster mass within the sphere of radius $R_{500}^X = 1110$ kpc. The concentration c is related to the mass by the relation from Duffy et al. (2008) derived from the analysis of cosmological simulations without baryons. The gray cross marks the cluster mass at which the Einstein radius coincides with the circumference radius Θ_{arc} . When estimating the uncertainty in the mass, we took into account only the error in Θ_{arc} . The vertical dashed line and the shaded region indicate the mass estimate for the cluster SRGe CL2305.2–2248 from SRG/eROSITA data.

gravitational potential in the central part of the cluster and, as a consequence, the mass estimate from strong lensing may turn out to be sensitive to the contribution of central galaxies and, possibly, hot gas to the density profile in the cluster. As numerical simulations show, the inclusion of baryons can indeed change significantly the density profile in the central region of the cluster (see, e.g.,

Table 3. Mass estimates for the cluster SRGe CL2305.2–2248 from X-ray and microwave observations and strong lensing

Parameter	$M_{500}, 10^{14} M_{\odot}$	Source
eROSITA	9.0 ± 2.6	Burenin et al. (2021)
ACT	9.2 ± 1.5	Hilton et al. (2021)
SPT	7.4 ± 0.8	Bleem et al. (2020)
Strong lensing	4.9 ± 0.7	This paper

Henson et al. 2017; Shirasaki et al. 2018), mainly through cooling and “adiabatic compression” (see, e.g., Gnedin et al. 2004). These effects can be partly taken into account by retaining the radial profile as in Eq. (2), but changing the concentration c compared to the numerical simulations without baryons. Above we obtained an estimate for the cluster mass by assuming that the concentration is expressed via the halo mass according to the relation from Duffy et al. (2008). However, the observations of strong and weak lensing of several well-studied clusters from the CLASH sample (Merten et al. 2015) give noticeably higher values of c than those predicted by the calculations of Duffy et al. (2008), which are based on cosmological simulations including only dark matter. If the concentration is fixed at a value twice the predicted one from Duffy et al. (2008), then the halo mass estimate is $M_{200} = 2.6 \times 10^{14} M_{\odot}$, $c = 8.3$, $M_{500} = 2.1 \times 10^{14} M_{\odot}$, $M(<R_{500}^X) = 2.8 \times 10^{14} M_{\odot}$. Thus, there is a noticeable uncertainty when extrapolating from $R_{\text{Ein}} = 72$ kpc to large radii ~ 1000 kpc, because the actual total density profiles of galaxy clusters can be considerably more complex than those predicted by numerical cluster

formation simulations without baryons and in view of the possible deviations from spherical symmetry.

DISCUSSION

The massive galaxy cluster SRGe CL2305.2-2248 at a redshift $z \simeq 0.76$ is a very rare object in the observable Universe. Its mass estimated from X-ray observations and the Sunyaev–Zeldovich effect, $M_{500} \sim 9 \times 10^{14} M_{\odot}$, is comparable to the mass of the cluster El Gordo. A total of ~ 10 so massive clusters at redshifts $z > 0.7$ in the entire sky is expected within the standard Λ CDM cosmological model. In this paper we investigated the deep direct images of the SRGe CL2305.2–2248 field obtained at the Russian–Turkish 1.5-m telescope (RTT-150) within the ground support of the X-ray survey with the eROSITA telescope onboard the SRG space observatory. Based on RTT-150 images and high-spatial-resolution images from the open Hubble Space Telescope (HST) archive, we selected probable gravitationally lensed sources, with the giant arc near the brightest cluster galaxies being also among them. We obtained a photometric redshift estimate for the arc, $z_S = 2.44 \pm 0.07$. The arc and several other lensed images lie virtually on one circumference with a radius of 9.8 ± 1.3 arcsec, which suggested a spherical symmetry of the lens and provided a direct measurement of the mass within the cylinder with a radius equal to the radius of the circumference (=the Einstein radius R_{Ein}). An extrapolation of the mass measurements based on strong lensing using the approximation of an isothermal sphere or the Navarro–Frenk–White profile for a reasonable range of concentrations c leads to M_{500} estimates lower than the estimate from the $M - L_X$ relation approximately by a factor of 1.5–3. Values of c that are well below the typical ones for relaxed clusters are required to reconcile these estimates. A possible explanation is a merger of clusters that led to a flatter mass distribution in the central part of the cluster. The presence of two massive galaxies at the center may also argue for this hypothesis. Another explanation can be a peculiarly high X-ray luminosity of this cluster. In principle, the luminosity can increase noticeably at certain merger phases. Consequently, the merger effect can also simultaneously lead to an overestimation of the luminosity and an underestimation of the concentration c . Detailed X-ray and microwave observations are needed for the dynamical state of the cluster to be reliably determined. The construction of an accurate lens model by the strong and weak lensing methods will also make it possible to draw conclusions as to whether we observe one massive cluster or a merger of several clusters and to estimate the halo mass irrespective of the dynamical

state. However, this requires measuring/estimating the redshifts of a large number of sources and measuring the elongation of background objects (for weak lensing).

APPENDIX

The analytical expressions describing the positions of tangential arcs in a spherically symmetric gravitationally lensed system, in which the lens density profile is described by the Navarro–Frenk–White profile, are presented in Bartelmann (1996). The properties of axisymmetric gravitational lenses are determined by their surface density $\kappa(x) = \Sigma(x)/\Sigma_{\text{cr}}$, where

$$\Sigma_{\text{cr}} = \frac{c^2}{4\pi G} \frac{D_s}{D_d D_{\text{ds}}}, \quad (4)$$

x is the coordinate along the radius in units of R_s , c is the speed of light, G is the gravitational constant, D_d and D_s are the angular diameter distances from the observer to the lens and the source, respectively, and D_{ds} is the angular diameter distance from the lens to the source. The mass within a circle of radius x is specified by the expression

$$m(x) \equiv 2 \int_0^x dy y \kappa(y). \quad (5)$$

In the case of spherically symmetric lenses, source images in the form of tangential arcs arise close to the tangential critical curve defined by the condition $m(x) = x^2$. The dimensionless surface density

$$\kappa(x) = 2\kappa_s \frac{f(x)}{x^2 - 1}, \quad (6)$$

where $\kappa_s \equiv \rho_s r_s \Sigma_{\text{cr}}^{-1}$, corresponds to the volume density $\rho(r)$ defined by Eq. (2). The dimensionless mass $m(x)$ is specified by the expression

$$m(x) = 4\kappa_s g(x), \quad (7)$$

where

$$g(x) = \ln \frac{x}{2} + \begin{cases} \frac{2}{\sqrt{x^2 - 1}} \arctan \sqrt{\frac{x-1}{x+1}}, & x > 1 \\ \frac{2}{\sqrt{1-x^2}} \operatorname{arctanh} \sqrt{\frac{1-x}{1+x}}, & x < 1 \\ 1, & x = 1. \end{cases} \quad (8)$$

ACKNOWLEDGMENTS

This study is based on observations with the eROSITA telescope onboard the SRG observatory. The SRG observatory was built by Roskosmos in the interests of the Russian Academy of Sciences represented by the Space Research Institute (IKI) within the framework of the Russian Federal Space Program, with the participation of the Deutsches Zentrum für Luft- und Raumfahrt (DLR). The SRG/eROSITA X-ray telescope was built by a consortium of German institutes led by MPE, and supported by DLR. The SRG spacecraft was designed, built, launched and is operated by the Lavochkin Association and its subcontractors. The science data are downlinked via the Deep Space Network Antennae in Bear Lakes, Ussurijsk, and Baykonur, funded by Roskosmos. The eROSITA data used in this paper were processed with the eSASS software developed by the German eROSITA consortium and the proprietary data reduction and analysis software developed by the Russian eROSITA Consortium. We are grateful to TÜBITAK, the Space Research Institute, the Kazan Federal University, and the Academy of Sciences of Tatarstan for their partial support in using the Russian–Turkish 1.5-m telescope (RTT-150) in Antalya.

This study is based on observations made with the NASA/ESA Hubble Space Telescope and obtained from the Hubble Legacy Archive, which is a collaboration between the Space Telescope Science Institute (STScI/NASA), the Space Telescope European Coordinating Facility (ST-ECF/ESAC/ESA), and the Canadian Astronomy Data Centre (CADC/NRC/CSA).

FUNDING

I.F. Bikmaev, R.A. Burenin, and S.N. Dodonov were supported by the Russian Science Foundation (project no. 21-12-00210). A.A. Starobinsky was supported in part by the Ministry of Education and Science of the Russian Federation (project no. 0033-2019-0005).

REFERENCES

1. M. Bartelmann, *Astron. Astrophys.* **313**, 697 (1996).
2. L. E. Bleem, S. Bocquet, B. Stalder, M. D. Gladders, P. A. R. Ade, S. W. Allen, et al., *Astrophys. J. Suppl. Ser.* **247**, 25 (2020).
3. R. A. Burenin, I. F. Bikmaev, M. R. Gil'fanov, A. A. Grokhovskaya, S. N. Dodonov, M. V. Eseevich, I. A. Zaznobin, E. N. Irtuganov, N. S. Lyskova, P. S. Medvedev, A. V. Meshcheryakov, A. V. Moiseev, S. Yu. Sazonov, A. A. Starobinskii, R. A. Syunyaev, et al., *Astron. Lett.* **47**, 443 (2021).
4. H. Dahle, N. Aghanim, L. Guennou, P. Hudelot, R. Kneissl, E. Pointecouteau, et al., *Astron. Astrophys.* **590**, L4 (2016).
5. A. R. Duffy, J. Schaye, S. T. Kay, and C. Dalla Vecchia, *Mon. Not. R. Astron. Soc.* **390**, L64 (2008).
6. J. Einasto, *Tr. Astrofiz. Inst. Alma-Ata* **5**, 87 (1965).
7. O. Y. Gnedin, A. V. Kravtsov, A. A. Klypin, and D. Nagai, *Astrophys. J.* **616**, 16 (2004).
8. M. A. Henson, D. J. Barnes, S. T. Kay, I. G. McCarthy, and J. Schaye, *Mon. Not. R. Astron. Soc.* **465**, 3361 (2017).
9. M. Hilton, C. Sifón, S. Naess, M. Madhavacheril, M. Oguri, E. Rozo, et al., *Astrophys. J. Suppl. Ser.* **253**, 3 (2021).
10. N. Lyskova, E. Churazov, and T. Naab, *Mon. Not. R. Astron. Soc.* **475**, 2403 (2018).
11. J. Merten, M. Meneghetti, M. Postman, K. Umetsu, A. Zitrin, E. Medezinski, et al., *Astrophys. J.* **806**, 4 (2015).
12. J. F. Navarro, C. S. Frenk, and S. D. M. White, *Astrophys. J.* **462**, 563 (1996).
13. P. Predehl, R. Andritschke, V. Arefiev, V. Babushkin, O. Batanov, W. Becker, H. Becker, H. Boehringer, et al., *Astron. Astrophys.* **647**, A1 (2021).
14. M. Shirasaki, E. T. Lau, and D. Nagai, *Mon. Not. R. Astron. Soc.* **477**, 2804 (2018).
15. R. Sunyaev, V. Arefiev, V. Babushkin, V. Bogomolov, K. Borisov, M. Buntov, H. Brunner, R. Burenin, et al., *Astron. Astrophys.* **656**, A132 (2021).
16. J. A. Smith, D. L. Tucker, S. Kent, M. W. Richmond, M. Fukugita, T. Ichikawa, et al., *Astron. J.* **123**, 2121 (2002).
17. B. C. Whitmore, S. S. Allam, T. Budavari, S. Casertano, R. A. Downes, T. Donaldson, et al., *Astron. J.* **151**, 134 (2016).

Translated by V. Astakhov